

Title: Self-regulating gene therapy ameliorates phenotypes and overcomes gene dosage sensitivity in a mouse model of Rett syndrome

Authors: Paul D. Ross^{1†}, Kamal K.E. Gadalla^{1†‡}, Sophie R. Thomson¹, Jim Selfridge¹, Noha G. Bahey^{1‡}, Juliana Benito², Suzanne R. Burstein², Rachel McMinn², Brad Bolon³, Ralph D. Hector^{1†}, Stuart R. Cobb^{1,2*}

Affiliations:

¹Simons Initiative for the Developing Brain, Centre for Discovery Brain Sciences, University of Edinburgh; Edinburgh, EH8 9XD, United Kingdom.

²Neurogene Inc.; New York, NY 10011, USA.

³GEMpath, Inc., Longmont, CO 805014, USA

[†]These authors contributed equally to this work

[‡]Current address: School of Science & Technology, Nottingham Trent University; Nottingham, NG1 4FQ, United Kingdom

*Corresponding author: S.R.C., stuart.cobb@ed.ac.uk

OVERLINE: GENE THERAPY

One Sentence Summary:

A gene therapy construct for Rett syndrome includes a self-regulating, miRNA-based feed-forward loop to prevent overexpression-related toxicity.

Editor's Summary:

Abstract: Conventional methods of gene transfer lead to inconsistent transgene expression within cells. This variability can be problematic, particularly in conditions like Rett syndrome (RTT), a neurological disorder caused by mutations in the *MECP2* (methyl-CpG binding protein 2) gene, because overexpression of *MECP2* can also cause adverse effects. To address these challenges, we devised a gene regulation system called Expression Attenuation via Construct Tuning (EXACT), which employs a self-contained, microRNA-based feed-forward loop that not only ensures more consistent transgene expression but also protects against excessive expression. Through cell-based screening assays, we demonstrated the ability of the EXACT circuit to modulate the expression of full-length human MeCP2. Compared to a conventional construct, an EXACT-*MECP2* construct exhibited a narrower range of cellular protein expression. Furthermore, the degree of regulation by the EXACT circuit increased with higher transgene doses in vitro and in wild-type mice and mice modeling RTT. Based on cellular and in vivo testing, we identified an optimal configuration for the adeno-associated virus serotype 9 (AAV9) construct for self-regulated *MECP2* gene therapy, designated NGN-401. Delivery of NGN-401 to neonatal male *Mecp2*^{-y} hemizygous mice via intracerebroventricular injection resulted in prolonged survival and amelioration of RTT-like phenotypes compared to vehicle-treated animals. NGN-401 was also well tolerated by female *Mecp2*^{+/-} mice and healthy nonhuman primates, in contrast to a conventional construct, which caused toxicity. The results from this study underpin a first-in-human pediatric study of NGN-401 in RTT (ClinicalTrials.gov, NCT05898620).

INTRODUCTION

Rett syndrome (RTT) is a severe neurodevelopmental disorder caused by loss-of function variants in the X-linked *MECP2* gene (1), encoding methyl CpG binding protein 2 (MeCP2) (2, 3), a nuclear protein expressed in the brain and other tissues. The disease occurs primarily in females who are heterozygous for the pathogenic mutation and affects about 1 in 10,000 females worldwide (4).

Individuals with RTT display apparently normal postnatal development followed by developmental delay between 6 and 18 months (5). This is followed by regression, leading to progressive loss of acquired skills in areas such as gross and fine motor skills and communication (6). Regression is defined by a loss of purposeful hand use and spoken language, with the development of gait abnormalities and hand stereotypies (7). Additional disease manifestations include seizures, as well as breathing abnormalities and gastrointestinal (GI) dysmotility. After this period of regression, typically by age 3, patients enter a phase of relative stability, where regression generally ceases (6). Patients begin to show further physical decline during adolescence and adulthood with further motor deterioration, developing rigidity, spasticity, dystonia, and scoliosis (6).

Despite the recent approval of the synthetic peptide trofinetide for treating symptoms of RTT (8), there are currently no approved treatments targeting the root cause of RTT, highlighting an unmet clinical need. Considering its monogenic etiology and the requirement for MeCP2 throughout life, gene therapy has emerged as an attractive treatment option for RTT. Moreover, gene therapy for RTT is particularly appealing because affected neurons remain viable (9) for potential restoration of function by a therapeutic transgene cassette. However,

although a deficiency of functional MeCP2, especially within the nervous system, drives the pathophysiology of RTT (10), excessive expression of MeCP2 is also damaging as highlighted in patients with *MECP2* duplication syndrome, where overexpression of MeCP2 from birth leads to severe intellectual disability, motor delay, and seizures (11). Therefore, achieving appropriate MeCP2 expression is critical for normal physiology. Because most individuals with RTT are females who are heterozygous for *MECP2* mutations, where MeCP2 deficiency is restricted to a mosaic pattern of cells due to random X-chromosome inactivation, an optimal gene therapy approach for RTT would deliver therapeutic MeCP2 expression to deficient cells while avoiding detrimental effects resulting from expressing MeCP2 beyond tolerable limits.

Genetic rescue (gene reactivation) and knockout studies support a gene therapy approach to RTT but have also identified the key tissues to target and confirm the dose sensitivity of the disorder. Previous studies where *MECP2* was selectively silenced in either the nervous system or peripheral tissues of mouse models have convincingly demonstrated that MeCP2 deficiency in the nervous system is the primary driver of RTT-like phenotypes and should thus be the main target for gene therapy (12-14). Using conditional alleles in mouse models, robust improvements in survival and reversal of neurological phenotypes were observed when the *Mecp2* locus was reactivated at various stages of postnatal development (15-17). However, toxicity resulting from genetic or gene therapy-induced MeCP2 overexpression in mice has been well-documented, leading to neurological deficits and lethality at high gene doses (18-22). High doses of adeno-associated virus (AAV) vectors expressing conventional (unregulated) *MECP2* transgene cassettes in mice also led to hepatotoxicity, emergence of non-RTT clinical signs, and early death (21-23), underscoring the need for constrained MeCP2 expression within a safe and tolerable window.

To address these challenges, we developed the Expression Attenuation via Construct Tuning (EXACT) technology built on the concept of using a microRNA (miRNA)-based incoherent feedforward loop to regulate transgene expression (24, 25). An incoherent feedforward loop is one in which the transgene, in this case *MECP2*, and a negative miRNA regulator are both expressed from the same promoter. The technology functions in a cell-autonomous manner and acts as a safety valve to ensure that protein expression is maintained within a safe range across transfected cells. This is important in AAV-based gene therapy where biodistribution is usually uneven, and cells receiving a high vector load are susceptible to superinfection-mediated transgene overexpression (26).

The objective of this study was to develop an optimized, self-regulated *MECP2* transgene and evaluate its potential as a gene therapy in RTT. Data from this study were part of Investigational New Drug (IND)-enabling nonclinical studies to advance this investigational gene therapy (NGN-401) into an ongoing Phase 1/2 clinical trial for female children with RTT (ClinicalTrials.gov, NCT05898620).

RESULTS

In vitro proof-of-concept studies of EXACT-*MECP2* plasmids

The EXACT gene therapy cassette comprises a single promoter driving expression of a full-length human *MECP2* transgene and a unique, non-naturally occurring, miRNA sequence

(designated EXACT1) generated from an embedded miRNA scaffold (**Fig. 1A**). This miRNA was designed to selectively regulate the transgene by binding fully complementary recognition sites, exclusive to the 3' untranslated region (3'UTR) of the transgene mRNA and avoiding off-target gene regulation.

To demonstrate the ability of the EXACT platform to regulate expression of an exogenous gene, we constructed plasmids containing the full-length human *MECP2* transgene fused to an mNeonGreen reporter where one plasmid contained the EXACT1 binding sites and the other did not. A second transcriptional unit on the same plasmid expressing the fluorescent marker, mRuby, was used to monitor the amount of construct delivered to each cell (as a surrogate for cellular dose / vector copy number) (**Fig. 1B**). The plasmids were transfected into HEK293A cells and after 48 h, flow cytometry was used to assess the effect of the EXACT1 miRNA circuit on MeCP2 protein expression. The EXACT construct, containing binding sites for the EXACT1 miRNA, reduced MeCP2 abundance compared to a control construct without the EXACT regulatory circuit, yielding a narrower range of protein expression across a wide range of plasmid dosage (**Fig. 1C**). To determine if the circuit could be tuned to achieve different degrees of regulation, a series of modified circuits were designed, including changing the number of EXACT1 binding sites in the 3'UTR of *MECP2*, including a mismatch in the center of the EXACT1 binding site, or by changing the intron used to express EXACT1. The different constructs were then transfected into HEK293A cells and assessed by flow cytometry. The data for each construct were used to generate cumulative probability plots (**Fig. 1D**), where the y-axis represents the cumulative probability of observing a given level of transgene expression (mNeonGreen fluorescence) or lower, indicating transgene expression. The unregulated control construct showed a broader range of transgene expression, whereas constructs with multiple EXACT binding sites demonstrated a narrower range of expression, with a plateau at three binding sites and fewer binding sites in the middle. These data demonstrated that EXACT imparted regulation of transgene expression in vitro. Modifications to this circuit led to intermediate degrees of regulation, highlighting that the circuit is tunable.

In vivo proof-of-concept studies of EXACT-MECP2 AAV vectors

To determine whether EXACT-*MECP2* constructs were able to provide the desired therapeutic benefit while preventing transgene-related toxicity in vivo, we performed an initial study in *Mecp2*^{-y} mice (12). AAV9 vectors were generated by packaging either a conventional transgene cassette utilizing the cytomegalovirus (CMV) enhancer/ chicken beta-actin (CBA) promoter driving expression of a full-length human *MECP2_e1* transgene or an equivalent but EXACT-regulated construct (**Fig. 2A**). *Mecp2*^{-y} mice were dosed with 3.0×10^{11} vector genomes (vg) at P0-2 via intracerebroventricular (ICV) administration and monitored for 30 weeks post-injection. The EXACT-regulated vector extended survival relative to vehicle-treated *Mecp2*^{-y} controls, whereas the conventional construct led to reduced survival relative to EXACT-treated and control mice (**Fig. 2B**). Expression analysis in the motor cortex, showed more constrained transgene expression in EXACT-treated mice compared to mice treated with the conventional vector (**Fig. 2C and fig. S1** for treated *Mecp2*^{-y} and WT mice, respectively).

Lead construct selection and mouse efficacy studies

We next compared constructs to identify a configuration that would provide more efficacious but constrained expression of MeCP2 protein. We designed a series of constructs aimed at achieving differential regulation of protein expression by systematically modifying individual elements of the regulatory circuit. These modifications included: (i) changing the intron in which the miRNA circuit is embedded from the original Efla intron to the small synthetic

MINX intron, which we previously showed in vitro to alter transgene expression levels (see **Fig. 1D**); (ii) the addition of a previously published shortened Woodchuck Hepatitis Virus Posttranscriptional Regulatory Element (WPRES) stability element (27) to enhance mRNA stability and increase transgene expression; (iii) single-base mutations to the miRNA binding sites at either position 14 (m1) or 20 (m2) which would impact seed sequence binding of the miRNA and would be expected to reduce the level of miRNA knockdown; and (iv) changing the EXACT miRNA sequence to alternative sequences (EXACT2 and EXACT3) (**Fig. 3A**). *Mecp2^{-y}* mice were then dosed by ICV administration of vector (3.0×10^{11} total vg per animal) or vehicle at P0-1 and monitored for survival. All constructs tested led to a marked extension of survival with the most effective construct, AAV9-RTT254, increasing median survival to 37 weeks compared to 9 weeks in the vehicle-treated control group (**Fig. 3B**).

AAV9-RTT254, hereafter known as NGN-401, was therefore adopted as our lead candidate and further evaluated in vivo for efficacy, safety and tolerability, and protein expression. We continued to utilize ICV delivery as the route of administration to maximize vector biodistribution to the nervous system. In addition to the 3.0×10^{11} total vg dose (1.9×10^{12} vg/g brain dose) already tested, *Mecp2^{-y}* mice were also treated with a lower dose of 1.0×10^{11} total vg/mouse (6.3×10^{11} vg/g brain) (**Fig. 4A**). Both doses of NGN-401 extended survival, with the low-dose group achieving a median survival of 23 weeks and the high-dose group achieving a median survival of 37 weeks, compared to 9 weeks in the vehicle control group (**Fig. 4B**).

Treated animals in both dosage groups also experienced a marked amelioration in RTT-like phenotypes as assessed by a clinical score that reflects the summation of individual scores from six parameters evaluated (mobility, gait, hind limb clasping, tremor, breathing, and general condition) (See Materials and Methods; **Fig. 4C**; **table S1**). Animals were also assessed for bodyweight (**Fig. 4D**). Scores for translationally relevant parameters, including mobility and gait were improved with NGN-401 (**fig. S2, A and B**). NGN-401 treatment also improved breathing scores, another translationally relevant measure, through reduced frequency of observable apnea (**fig. S2C**; **table S1**). Other observable phenotypes, including tremor, hindlimb clasping, and general condition, were also improved with NGN-401 treatment (**fig. S2, D to F**). In contrast, vehicle-treated *Mecp2^{-y}* mice developed a rapid rise in clinical scores to maximal severity for mobility, gait, and hindlimb clasping parameters, exhibiting a severe loss of locomotion and clasping in hindlimbs (**fig. S2, A and B, E**).

In the cerebral cortex, where high vector transduction was observed after ICV delivery, vector-derived MeCP2 was detected at expression close to those observed in vehicle-treated wild-type animals (expression assessed 8 weeks after dosing; **Fig. 4E and fig. S3**). Importantly, although vector biodistribution increased with dose (**Fig. 4F**), MeCP2 protein expression did not increase proportionately (**Fig. 4E**), illustrating that EXACT does regulate MeCP2 expression, even when viral copy numbers per cell are increased.

NGN-401 tolerability studies in female *Mecp2^{+/-}* mice and wild-type juvenile nonhuman primates

The ability of NGN-401 to limit MeCP2 overexpression was further evaluated in female *Mecp2^{+/-}* mice to model the genotype of most patients with RTT. NGN-401 tolerability was compared to an unregulated vector with the same CMV/CBA promoter driving expression of wild-type human *MECP2*. *Mecp2^{+/-}* mice were dosed at P0-2 by ICV administration at 1.0×10^{11} , 3.0×10^{11} , or 7.4×10^{11} vg of NGN-401 or the unregulated vector. The 7.4×10^{11} vg dose represented the maximum feasible dose in the study based on AAV titer and injection volume constraints. Survival, toxicity and body weights were evaluated over 26 weeks post-injection (**Fig. 5, A to C**). Overt toxicity was assessed using a scoring system that was

developed in our laboratory and is described in detail in **table S2**. Severe toxicity was observed in mice treated with the unregulated *MECP2* vector, at both the 1.0×10^{11} and 3.0×10^{11} vg doses with either lethality or animals having reached the humane endpoint for euthanasia occurring by 3 weeks post-dosing (**Fig. 5, A and B**). Therefore, for ethical reasons, mice were not injected with the unregulated construct at the maximum dose of 7.4×10^{11} vg. In contrast, NGN-401 was well-tolerated in *Mecp2*^{+/-} mice at all doses tested, including the highest dose of 7.4×10^{11} vg (**Fig. 5, A to C**). At both the 1.0×10^{11} and 3.0×10^{11} vg doses, NGN-401 showed no adverse effect on survival (**Fig. 5A**) and no observable toxicity, maintaining an average toxicity score near 0 throughout the study (**Fig. 5B; table S2**). At 7.4×10^{11} vg, NGN-401-treated mice showed an average toxicity score of 1, due to the presence of mild hind limb claspings that was not progressive. A masked ('blinded') histopathological assessment was conducted (performed by B.B., an American College of Veterinary Pathologists (ACVP)/Fellowship Examination of The Royal College of Pathologists (FRCPath)-certified veterinary pathologist) covering neural and peripheral tissues from mice at 8 and 26 weeks, which did not find evidence of NGN-401-related neuropathological changes (**table S3**), suggesting that the MeCP2 expression achieved was well-tolerated in this model. Histopathological evaluation of liver did not reveal any NGN-401-related findings despite the presence of vector genome DNA (0.18 – 0.49 vg/diploid genome). *Mecp2*^{+/-} mice displayed an elevated body weight relative to wild-type controls, which appeared to be corrected with NGN-401 treatment at all doses tested.

MeCP2 abundance increased in the cerebral cortex of NGN-401-treated *Mecp2*^{+/-} females compared to vehicle-treated animals (**Fig. 5D and fig. S3**), but in a constrained and more attenuated manner relative to the increase in vector genome detected (**Fig. 5E**). In contrast, *Mecp2*^{+/-} mice treated with the same doses of unregulated *MECP2* vector showed MeCP2 abundances 15 to over 20 times higher than those seen in vehicle-treated wild-type mice (**Fig. 5D**).

As a path to clinical development, an initial tolerability and biodistribution study was conducted to evaluate ICV administration of NGN-401 in nonhuman primates (NHPs). *Cynomolgus* macaques (*Macaca fascicularis*) were used because *MECP2* is highly conserved across species, with >99% identity between human and macaque and MeCP2 protein is expressed in all cells (28). Before initiating these studies, EXACT regulation of MeCP2 was confirmed in vitro in cultured NHP-derived COS-7 cells. As expected, transfection with increased concentrations of plasmids containing NGN-401 expression cassette was accompanied by increased dampening of transgene mRNA expression (**fig. S4A**) and resulting protein abundance (**fig. S4B**).

In the NHP study, NGN-401 was compared to the unregulated *MECP2* vector. Juvenile cynomolgus macaques were treated once at 3.7×10^{13} or 1.1×10^{14} vg by ICV infusion (n=2 males and n=1 female per group, see the Materials and Methods for details of immunosuppression regimen). *MECP2* mRNA expression in key tissues, collected at 1-month post-dosing, from animals treated with the unregulated vector was more variable and several fold higher than in tissues from animals that received NGN-401 (**Fig. 5F**), providing evidence that EXACT regulates expression in a large animal model. Overall, NGN-401 was well-tolerated with no loss in body weight, and all treatment-related observations were expected outcomes of AAV9 delivery (26, 29, 30) and not NGN-401 toxicity. Specifically, transient serum chemistry changes, including elevated alanine aminotransferase (ALT) activity, resolved without intervention (see Data file S1). Test article-related microscopic observations in dorsal root ganglia and spinal cord (see table in Data file S1) were considered non-adverse due to their minimal or slight severity and lack of functional correlates.

Together, these data supported the safety of NGN-401 when administered to NHPs via a clinically relevant route of administration, at doses that bracket the human equivalent dose (ClinicalTrials.gov, NCT05898620).

Because peripheral nerve dysfunction and slowing of nerve conduction velocity (NCV) is a known feature to monitor in AAV gene therapy, we collected NCV measures at baseline and at 30 days post-treatment. NCV remained within the physiologically functional range for most NGN-401-treated animals, with one of six displaying sural NCV slowing. In contrast, 5 of 6 animals treated with the conventional gene therapy construct displayed slowing or complete loss of sural nerve response at 30 days post-treatment (see Data file S1).

A final safety consideration represents the potential for off-target effects of EXACT1 miRNA circuit. Although the EXACT1 miRNA contains no predicted close matches within the human transcriptome, we extended the assessment of EXACT1 miRNA using a combination of *in silico* and RNA sequencing (RNA-seq) analyses (fig. S5). Overall, no significant off-target effects were observed across multiple cell lines representing different tissue types when EXACT1 miRNA was overexpressed (table S4).

DISCUSSION

Gene dosage-sensitive conditions such as RTT are not well suited for conventional gene therapy. The EXACT technology represents a miniaturized control circuit that is self-contained within the gene therapy cassette and enables a cell-by-cell tuning of therapeutic transgene expression. This in-built system provides the ability to deliver an effective but controlled therapeutic payload that achieves superior performance and control over conventional transgene cassettes. In this, the EXACT approach overcomes the fundamental challenges related to variable payload delivery and tissue uptake inherent with AAV vector delivery. EXACT harnesses the cell's ability to regulate transcript expression through miRNA processing, but it does not rely on native miRNAs that vary by cell type, tissue, and species. RTT is just one of many gene dosage indications that represent a challenge for conventional gene therapy. For example, overexpression of a transgene has been problematic in other monogenic disorders, such as Spinal Muscular Atrophy and Friedreich's Ataxia (26, 31, 32). Through its modular design and tunability, EXACT may provide a controlled gene transfer solution in other indications where progress in gene therapy has been hindered by uncontrolled expression challenges.

This study demonstrated a marked dose-dependent survival benefit and amelioration of disease-relevant phenotypes in *Mecp2*^{-y} mice treated with NGN-401. The survival benefit afforded by NGN-401 resembles that seen in a conditional mouse model undergoing genetic rescue, where *Mecp2* is reactivated at its endogenous locus and under native regulation (16). Early dosing in this severe model is necessary due to both the early morbidity that makes ICV surgery not readily feasible at later ages (33-38) and the time taken for vector-derived protein expression (39-41). Taken together, these data suggest that NGN-401 may offer therapeutic benefit if delivered to enough relevant cells in a human patient.

Several preclinical studies have highlighted the potential for gene therapy in RTT (21, 22, 42-49). However persistent concerns remain around MeCP2 toxicity and the narrow therapeutic window, which have led to adverse outcomes, including lethality as well as liver and CNS toxicity in rodent studies (21, 23, 44). In this study, mice treated with a vector containing a

conventional gene therapy cassette exhibited similar severe outcomes associated with MeCP2 overexpression, but those treated with a vector containing a cassette controlled by self-regulating EXACT technology did not. *Mecp2*^{+/-} mice treated with a maximum feasible dose, well beyond the maximal clinically feasible dose, and representing a >6-fold greater than the 1x10¹⁵ vg dose in the ongoing Phase 1/2 clinical trial, did not manifest any overt adverse effects beyond nonprogressive hindlimb clasping. The correction of bodyweight with NGN-401 in *Mecp2*^{+/-} mice mirrors the normalization seen by Guy *et al.* (15) following genetic reactivation of a STOP allele in a conditional reactivation model. NGN-401 also demonstrated good tolerability in NHP studies, supporting its ability to avoid variable and high transgene expression and overt toxicity in a translationally relevant species.

In the current study and the ongoing NGN-401 Phase 1/2 clinical trial, NGN-401 was administered by ICV infusion. Conditional genetics studies underscore that MeCP2 deficiency within the nervous system is the primary driver of RTT-like phenotypes (13, 50). Hence, it is crucial to optimize delivery to key areas of the brain that underpin RTT pathobiology. Although alternative systemic and intrathecal routes of AAV administration have been explored in RTT mouse models and at different ages, they have yielded limited brain biodistribution, brain protein expression, and efficacy (21, 22, 42, 46, 47). Moreover, systemic and intrathecal administration have demonstrated low biodistribution to the brain in large animal species, including humans (51). ICV administration of NGN-401 allows for safe dose escalation to maximize biodistribution across key brain structures without surpassing safety thresholds.

Other approaches aimed at mitigating the potential for MeCP2 overexpression that have been used include using weak native promoter fragments and regulatory elements (21, 22, 45), expressing unstable or hypomorphic forms of MeCP2 (28, 44), weakening expression through detecting naturally occurring miRNAs (21, 46, 47), or a combination thereof. However, these approaches do not offer proportional regulation in relation to the amount of gene therapy delivered to a cell or tissue and have not been shown to produce a widening of the therapeutic window.

Various DNA- and RNA-level editing approaches under exploration for RTT hold promise for addressing challenges related to *MECP2* copy number and durability (52-54). However, these strategies face substantial hurdles in delivery, efficiency, and selectivity. For instance, gene editing payloads are often large, necessitating vector splitting, which can impact delivery efficiency and efficacy. In addition, most editing platforms are designed to correct only a single or a limited subset of RTT-causing mutations, making it difficult to develop a broadly applicable therapy for the diverse range of pathogenic *MECP2* variants that occur throughout the gene.

Our study has several limitations. Firstly, the mouse studies focused on early neonatal dosing that represents intervention at an earlier developmental timepoint relative to the pediatric population in the clinical trial. This was necessitated by technical limitations with the mouse line as detailed above. A second limitation relates to the adoption of a refined observational scoring system. Although this provided a more granular assessment of MeCP2 deficiency phenotypes than that used previously, it relied on observational measures that were not readily captured by video or automation. A third limitation of the study was the restricted presentation of cellular MeCP2 analysis and the relative focus on bulk sample analysis in the animal studies. We have nevertheless shown regulation of *MECP2* expression and MeCP2 abundance by EXACT in human and NHP cells and in mouse and NHP brains. Future studies will explore the application of the EXACT technology in other dosage-sensitive indications.

to demonstrate its broad applicability to other disorders that are not currently well suited for conventional gene therapy.

In conclusion, we presented the development and characterization of a self-regulating gene therapy for treating RTT. Incorporating EXACT regulatory elements into NGN-401 led to modulated expression of human *MECP2* and enhanced efficacy and tolerability in animal studies, paving the way for a Phase 1/2 clinical trial in female pediatric patients with RTT (ClinicalTrials.gov, NCT05898620).

MATERIALS AND METHODS

Study design

The primary hypothesis of this study was that a miRNA-based regulatory circuit (EXACT constructs) could safely constrain *MECP2* transgene expression within therapeutic levels suitable for RTT gene therapy. To test this hypothesis, EXACT constructs were first screened in a cell-based fluorescent reporter assay, where candidate *MECP2* transgenes were fused to a fluorescent reporter. A second fluorescent reporter expressed from a separate transcriptional unit served as a surrogate measure for gene dosage. The efficacy of selected EXACT constructs was subsequently assessed in vivo using the *Mecp2*^{-y} mouse model, a well-established RTT model, following neonatal ICV administration (12). Primary efficacy endpoints included survival, body weight, and clinical scores assessing RTT-like phenotypes throughout the study duration. Tolerability was evaluated in a female *Mecp2*^{+/-} mosaic mouse model, as the sex, genotype, and mosaicism of MeCP2 expression in these animals closely resemble the genetic characteristics observed in female RTT patients. Further tolerability assessments were performed in juvenile cynomolgus macaques (*Macaca fascicularis*) following unilateral ICV injection.

All animal experiments were conducted in accordance with the European Communities Council Directive (86/609/EEC) and approved under a project license granted by the UK Animals (Scientific Procedures) Act 1986. Investigators analyzing experimental outcomes were blinded to both animal genotype and treatment groups. Animal sample sizes were determined based on prior experience from similar gene therapy studies, providing sufficient power to discriminate therapeutic effects. Animals were excluded from the study only if they developed non-treatment-related tail injuries or penile lesions requiring humane euthanasia (table S5). Flow cytometry (FACS), quantitative PCR (qPCR), and quantitative reverse transcription PCR (qRT-PCR) experiments were performed in triplicate, whereas Western blot experiments were conducted once. The exact numbers of animals used per experiment are indicated in the figure legends.

Animals

All experiments were carried out in accordance with the European Communities Council Directive (86/609/EEC) and within project license terms under the UK Animals (Scientific Procedures) Act 1986. The B6.129P2(C)-*Mecp2*^{tml.1Bird/J} (The Jackson Laboratory, stock # 003890) line was maintained on a mixed C57BL/6 CBA genetic background by crossing heterozygous females (*Mecp2*^{+/-}) with wild-type B6CBAF1 males from an external supplier. Experimental cohorts were generated by timed mating with copulation confirmed by the presence of a vaginal plug. Pregnancies were confirmed 15-17 days after mating, and visibly pregnant females were housed separately and monitored daily for litters. For inclusion in

neonate dosing studies, neonates were genotyped using a tissue biopsy taken at postnatal day 0 (P0). Mice were ear notched for identification and genotype confirmation at P14-21. To minimize potential study bias, mice were randomly assigned to different AAV9 and vehicle treatment groups. Appropriate sample sizes were determined based on previous studies performed by the group using these RTT mouse models.

Animals were housed in filter-capped cages positively ventilated with HEPA-filtered air. At weaning, experimental animals and controls were transferred to open-top cages. Animal rooms were illuminated by artificial fluorescent lighting and maintained on a 12 h light/dark cycle (7 am to 7 pm light). Room temperature and humidity were maintained at 20 ± 2 °C and 50 ± 15 %, respectively. Animal rooms received 20 air exchanges per h. All animals had *ad libitum* access to filtered, acidified tap water and standard rodent chow.

Constructs

In vitro reporter constructs expressing a human *MECP2_e1* transgene under control of an EXACT miRNA circuit were produced using the Extensible Mammalian Modular Assembly (EMMA) kit. The EMMA approach uses Golden-Gate cloning at the Edinburgh Genome Foundry for the modular assembly of mammalian expression vectors in a one-tube, one-step reaction using a library of compatible genetic parts (55). DNA fragments, containing individual genetic elements, were synthesized by GeneArt (Thermo Fisher Scientific). Clones were verified using fragment analysis and next-generation sequencing (NGS). In vitro constructs used to assess off-target effects of EXACT1 miRNA were modified versions of these reporter constructs, expressing EXACT1 miRNA and a mNeonGreen transgene but not expressing *MECP2*. As a control, a construct with the same promoter, transgene, and Simian virus 40 polyadenylation signal (SV40pA) but without the EXACT1 miRNA circuit was used. For in vivo constructs, DNA fragments containing a promoter, human *MECP2_e1* transgene, and SV40pA, plus or minus an EXACT miRNA circuit, were synthesized by GENEWIZ. Sequences for NGN-401 (RTT-254) and for the unregulated comparator construct are provided in Data file S2. Constructs were subsequently cloned into a baculovirus vector, V445-ss-pFB, by Virovek Inc. The resultant vector contained the gene therapy construct flanked by single-stranded AAV2 inverted terminal repeats (ITRs) and a Tn7L recognition sequence to make the vector compatible with Baculovirus AAV production. Cloning of the constructs was confirmed by Sanger sequencing prior to AAV production. The sizes of NGN-401 and the unregulated vector were 3594 bp and 3871 bp (including ITRs), respectively, and fell well within the ~4.8 kb packaging capacity of single-stranded AAV.

AAV9 viral vector production

AAV9 constructs used in these studies were generated using a Baculovirus Expression Vector System (BEVS)-based process, using *Spodoptera frugiperda* (Sf9) insect cells. The system employs two baculovirus vectors: one baculovirus vector encodes the Rep2 and Cap9 proteins (rBV-Rep2Cap9) and the other contains the transgene (rBV-*hMECP2*). The two rBV constructs were expanded and used to co-infect the Sf9 cells to generate the rAAV product, AAV9-RTT254 (NGN-401). The AAV9 material used in these studies was generated by Virovek Inc. using their standard AAV production process. The process uses high-density Sf9 cells infected with both baculovirus constructs (not plaque purified) at a predefined multiplicity of infection (MOI), and rAAV is harvested 3 days post-infection. During harvest, cells are chemically lysed using a detergent, and the culture treated with endonuclease (Benzonase) before filtration. Clarified lysate is purified using two rounds of CsCl gradient purification, following a de-salting step to remove any residual CsCl salt. The final product is formulated in phosphate-buffered saline (PBS) containing 0.001 % Poloxamer 188. Quantity

and quality of AAV9 material were assessed by digital droplet polymerase chain reaction (ddPCR) (table S6).

ddPCR analysis

A single-plex ddPCR assay targeting the CMV enhancer was used to determine the viral titer of AAV material for dosing. Encapsidated DNA from the rAAV was isolated with nonencapsidated DNA and vector capsids digested by DNase I and proteinase K, respectively. Samples were subjected to droplet generation to segregate viral genomes, then fragments of the viral genome were amplified by ddPCR with primers specific for the CMV enhancer sequence: CMV-F (5'-3'): GAC GTC AAT GGG TGG AGT AT; CMV-R (5'-3'): CCA TAA GGT CAT GTA CTG GG. Lastly, amplification signal was measured based on the signal produced by a CMV-specific probe that hybridizes to the amplicon: TGC CAG GCG GGC CAT TTA CCG TCA. Titers were calculated based on the proportion of positive and negative droplets, and titer was reported in vg/mL.

Cell culture and transfections

HEK293A, HepG2, SH-SY5Y, and COS7 cells (American Type Culture Collection [ATCC]) were maintained in Dulbecco's modified Eagle's medium (DMEM) with 4.5 g/L D-glucose supplemented with 10 % heat-inactivated fetal bovine serum (FBS), 2 mM L-glutamine, and 1× MEM nonessential amino acids solution (Thermo Fisher Scientific). Cells were subcultured every 2-3 days and seeded at 2×10^6 cells in T175 vented flasks (Greiner Bio-One). Cells were grown in a humidified incubator at 37 °C and 5 % CO₂.

For flow cytometry experiments, cells were cultured to 80-90 % confluency before the day of transfection, trypsinized (TrypLE™ Express, Life Technologies), and seeded into 96-well plates (Greiner Bio-One) coated with poly-L-ornithine (Sigma Aldrich) and fibronectin (Sigma Aldrich) at 8×10^3 cells per well. Cells were transfected using Lipofectamine 2000 (Life Technologies) following the manufacturer's protocol with 100 ng plasmid mixed with Opti-MEM (ThermoFisher Scientific) per well. For expression studies, COS7 cells were seeded in 24-well plates at 5×10^4 cells per well. Cells were transfected with equimolar ratios of plasmids and collected for RNA or protein extraction 48 h post-transfection.

Fluorescence-activated cell sorting (FACS) analysis

At 48 h post-transfection, cells were prepared for flow cytometry by removing the media, washing the cells with Dulbecco's PBS (DPBS; Life Technologies), and adding TrypLE™ (Life Technologies) for 3 min. Growth media was added, and the cells were resuspended and transferred into 1.5 mL tubes followed by centrifugation at $200 \times g$ for 5 min. Cell pellets were resuspended in DPBS into 5-mL FACS Falcon® tubes and kept on ice until flow acquisition. In total, 5,000 events were recorded per sample in triplicate using a BD LSRFortessa cell analyzer (BD Biosciences). Samples were sorted using a LSRFortessa SORP flow cytometer (Beckton Dickinson [BD] Immunocytometry Systems) equipped with 488 nm and 561 nm lasers running BD FACSDiva v8 software. An electronic acquisition gate was applied to the Forward/Side scatter plot to exclude debris from intact material. mNeonGreen reporter expression was detected following 488 nm excitation at emission between 530/30 nm. mRuby reporter expression was detected following 561 nm excitation at emission between 610/20 nm. At least 5,000 intact mRuby-positive cells were recorded for analysis. Aggregated material was excluded based on FSC Area versus Width plot profiles before subsequent analysis.

In vivo gene transfer and efficacy analysis

Mice were dosed at P0-2 via ICV injection. This age was selected as *Mecp2*^{-y} mice develop early pathological phenotypes that render them unlikely to recover from anesthesia and stereotactic ICV surgery required at later postnatal ages. Specifically, anesthetized (isoflurane) neonates were injected bilaterally (5 μ L per site; $1-7.4 \times 10^{11}$ vg/pup) with vector or vehicle (PBS + poloxamer) using a 30 G dental needle attached to a 50 μ L Hamilton syringe over a period of 30 s per injection site. The needle was kept in place for 60 s and then removed slowly over 30 s to minimize backflow of the injected vector particles. The injection sites were over the temporal cortex, $\sim 1-2$ mm lateral from the midline and ~ 2 mm rostral (anterior) to lambda, and the dose was delivered to an approximate depth of 2-3 mm. The injected pups were allowed to recover on a heated pad and then returned to the home cage, wrapped with the cage bedding to prevent maternal rejection. Dosing at this developmental period was selected as these mice develop a rapid and severe disease phenotype and several weeks are required to permit disease-modifying expression of the AAV-delivered transgene. Survival, body weight, and scores for RTT-like phenotypes were assessed throughout the study period from 4 weeks of age onwards.

RTT score

Disease phenotype was quantified using a refined RTT scoring system, a non-invasive observational clinical scoring system that grades and aggregates the severity of RTT-like phenotypes spanning multiple domains, including locomotor function, breathing, and general health (**Table S1**). This RTT score was developed based on a published mouse phenotypic scoring system (15) to provide more detailed and finer grain evaluation of multiple disease-relevant in-life phenotypes that are present in the model. Using this system, animals are given a score of 0-5 by a researcher (blinded to phenotype and treatment group) in each of six parameters: mobility, gait, hindlimb clasp, tremor, breathing, and general condition. A score of 0 signifies the phenotype of wild-type animals (i.e., 'normal'), and a score of 5 represents the most severe phenotype. The RTT score for any animal reflects the sum of the scores for the six traits with the aggregate ranging from 0-30 compared to the 0-12 points used in the previous scoring system. Humane endpoints were triggered by any of the following: (1) an aggregate score of ≥ 20 ; (2) a score of 5 in the individual tremor, breathing, or general condition phenotypes (red text); or (3) loss of $> 20\%$ of the maximum body weight.

MeCP2 overexpression toxicity score

For NGN-401-treated mice, MeCP2 overexpression toxicity was assessed weekly from P28 onwards using a 6-point scoring system developed as shown in **Table S2**. Mice treated with the unregulated vector died or reached a humane endpoint before planned initiation of toxicity scoring. Mice that reached the humane endpoint were scored for MeCP2 overexpression toxicity before culling.

Terminal procedures and tissue collection

Mice that survived to the end of each study or reached a humane endpoint were euthanized using an anesthetic overdose (pentobarbitone). Brain and selected peripheral organs were excised, snap-frozen in liquid nitrogen, and retained at $-80\text{ }^{\circ}\text{C}$ for further analysis.

Immunohistochemistry

Mice were terminally anaesthetized with pentobarbitone (50 mg, intraperitoneally) and perfused with 4% paraformaldehyde (in 0.1 M PBS) and post fixed for a further 48 h at $4\text{ }^{\circ}\text{C}$. Sections were obtained using a vibrating microtome (Leica VT1200; Leica) and processed for immunohistochemistry using anti-MeCP2 antibodies (Sigma M7443, 1:500) or anti-FLAG- (Sigma, F7425, 1:500 dilution) and fluorophore-conjugated secondary antibodies. Stained

sections were imaged using a Zeiss LSM800 confocal microscope. The scan parameters for quantitative analyses were set so that the highest signals were non-saturating. A minimum of six random fields were sampled per tissue for each subject. All image stacks captured were subsequently processed using ImageJ software; intensity was determined using QuPath software (56)

Western blot analysis

Snap-frozen tissues or transfected cells were homogenized in NE1 buffer (20 mM HEPES, 10 mM KCl, 1 mM MgCl₂, 0.1 % Triton X-100, 20 % glycerol, 0.5 mM DTT, Pierce Protease Inhibitor Tablet, EDTA-free [A32965, ThermoFisher Scientific]) in a Bead Mill 24 homogenizer (Fisher Scientific). Genomic DNA was removed with a benzonase digest (E1014, Merck) for 15 min at room temperature. Protein concentration was quantified using DC BioRad II (5000112, BioRad) in a microtiter plate using a FLUOstar Omega plate reader (BMG Labtech). Samples were diluted in one-third volume 4× Laemmli buffer (0.5 M Tris-HCl, 8 % SDS, 0.01 % bromophenol blue, 40 % glycerol, 10 % beta-mercaptoethanol) and denatured at 95 °C for 10 min before being storing at –80 °C. Protein samples (20 µg/lane) were resolved and transferred to nitrocellulose membranes (BioRad). Total protein was measured using Revert 700 Total Protein Stain (926-11010, LI-COR), and membranes were blocked in Intercept (TBS) Blocking buffer (927-60001, LI-COR) for 1 h at room temperature. Rabbit anti-MeCP2 primary antibody (S3456; Cell Signaling Technology; 1:1,000) was incubated at 4 °C overnight. Secondary antibodies (IRDye 800CW donkey anti-rabbit IgG secondary antibody [926-32213; LI-COR]; 1:10,000) were incubated for 1 h at room temperature before data were captured on a LI-COR Odyssey Classic. Western blots were replicated multiple times using 6-14 biological replicates per group (depending on group sizes). Data were analyzed using Image Studio Lite (LI-COR) and Microsoft Excel.

Vector DNA biodistribution

DNeasy Blood and Tissue Kit (69504, Qiagen) was used to extract DNA from snap-frozen tissues. Tissues were homogenized in buffer ATL + proteinase K as per manufacturer's instructions in a Bead Mill 24 (Fisher Scientific) for 20 seconds and incubated at 56 °C for 1 h before following manufacturer's instructions for DNA purification. DNA concentrations were measured using a Nanodrop 2000 (ThermoFisher Scientific). Vector copy number was determined using a Taqman absolute quantitative PCR (qPCR) assay targeting the WPRE3 sequence incorporated in the 3'UTR of the constructs used in this study. Known copy numbers of a linearized plasmid containing the WPRE3 sequence were used as a standard. qPCR was performed using Taqman Fast Advanced Master Mix (4444557, ThermoFisher Scientific) that included the following: forward and reverse primers at final concentrations of 900 nM (F, 5'-CTA TGT GGA TAC GCT GCT-3' and R, 5'-GGC AAG AAC TAA CCA GGA-3'), probe at a final concentration of 250 nM (/56-FAM/TCATGCTAT/ZEN/TGCTTCCCGTATGG/3IABkFQ/), and 100 ng DNA per well. Mouse beta-actin (*Actb*) copy numbers were determined using a SYBR Green qPCR assay targeting the endogenous *Actb* sequence. Known copy numbers of a linear gBlock DNA fragment (IDT) containing the *ActB* sequence were used as a standard. *Actb* qPCR was performed using the 2× Perfecta SYBR Green Fast Mix, ROX (Quantabio) that included the following: forward and reverse primers at final concentrations of 250 nM (F, 5'-AGC CAT GTA CGT AGC CAT CC-3' and R, 5'-CTC TCA GCT GTG GTG GTG AA-3'), and 100 ng DNA per well (the same test sample as used for the WPRE3 assay). Assays were performed using 3-6 biological replicates (depending on group sizes) and in technical triplicate. All plates were run on StepOne Plus (Applied Biosystems) using StepOne Software V2.3 (Applied Biosystems). Copy numbers per well were extrapolated from the standard curve

using Microsoft Excel, and vector genomes per diploid genome were calculated by normalizing WPRE3 copy number to *Actb* copy number.

qRT-PCR quantification

RNA was extracted from snap frozen tissue or transfected cells by homogenization in Qiazol (79306; Qiagen) following the manufacturer's instructions. RNA was reconstituted in 25 μ L nuclease-free water, and concentrations were measured using a Nanodrop 2000 (ThermoFisher Scientific). RNA quality was assessed using an Agilent TapeStation 4200 (Agilent Technologies). Genomic DNA was removed from RNA samples using RQ1 DNase (M6101, Promega) following the manufacturer's instructions. Conversion to cDNA was performed using 1 μ g RNA and VILO Superscript IV (11756050, ThermoFisher Scientific). After the cDNA was diluted 1:20 with nuclease-free water, vector-derived mRNA copy number was determined using absolute quantitative reverse transcription-PCR (qRT-PCR). Vector-derived transgene expression was determined using a Taqman absolute qRT-PCR assay targeting the WPRE3 sequence incorporated in the 3'UTR of the constructs used in this study. Known copy numbers of linearized plasmid containing the WPRE3 sequence were used as a standard. qRT-PCR was performed using Taqman Fast Advanced Master Mix (4444557, ThermoFisher Scientific) with the primers and probe described above. A final concentration of 12.5 ng cDNA was loaded per well. Assays were performed using 3-6 biological replicates (depending on group sizes) and in technical triplicate. Plates were run on a StepOne Plus system (Applied Biosystems) using StepOne software V2.3 (Applied Biosystems). WPRE3 copy numbers per well were extrapolated from the standard curve using Microsoft Excel.

Nonhuman primate studies

Evaluation of AAV9-RTT254 (NGN-401) and AAV9-hMECP2 in juvenile cynomolgus macaques (*Macaca fascicularis*, Asian origin, n=2 males and n=1 female per group) was sponsored by Neurogene Inc. and performed at Labcorp Early Development Laboratories Inc. All study procedures were in compliance with applicable animal welfare acts and were approved by the Labcorp (Madison, WI) Institutional Animal Care and Use Committee (Study 8467059). Animals were socially housed, provided water *ad libitum*, and offered Irradiated Certified Primate Diet #2955C (Envigo Certified LabDiet®). Environmental controls were set to maintain a temperature range of 20-26 °C, a relative

humidity range of 30-70 %, eight or greater air changes/h, and a 12-h light/12-h dark cycle. Animals received daily oral prednisolone (1 mg/kg) beginning 2 weeks prior to vector dosing throughout the duration of the study. This regimen was implemented to reduce immune response to the viral vector and reflects standard practice in the clinical setting for AAV gene therapy. Vectors were administered via a unilateral ICV injection of up to 1.3 mL and tissues were collected 1 month after dosing. Study assessments included clinical and neurobehavioral observation, body weight, food consumption, nerve conduction, clinical pathology, and anatomic pathology. Transgene mRNA expression was evaluated by qRT-PCR as described above.

Statistical analysis

Statistical analyses were performed with GraphPad Prism (version 10). Survival curves for the mouse efficacy and toxicity study were analyzed with the Log-rank (Mantel Cox) comparison of *Mecp2*^{-y} groups, excluding the wild-type group. Significant differences in median survival between each of the AAV-treated groups and the vehicle-treated group were tested with the Bonferroni correction as follows: the family-wise alpha level was set at 0.05 and divided by the number of pair-wise comparisons to obtain the Bonferroni-corrected alpha

value. The Log-rank (Mantel Cox) test was performed again for each of the pair-wise comparisons, and survival differences were deemed statistically significant based on the corrected alpha value. For Western blot and biodistribution data, groups were compared with unpaired t-tests or one-way analysis of variance (ANOVA) with Tukey's *post hoc* comparisons as appropriate. All graphs show mean \pm standard error of the mean (SEM).

List of Supplementary Materials

Figs. S1 to S5.

Tables S1 to S6.

Data files S1 to S4.

References and Notes

1. R. E. Amir, I. B. Van den Veyver, M. Wan, C. Q. Tran, U. Francke, H. Y. Zoghbi, Rett syndrome is caused by mutations in X-linked MECP2, encoding methyl-CpG-binding protein 2. *Nat Genet* **23**, 185-188 (1999).
2. J. D. Lewis, R. R. Meehan, W. J. Henzel, I. Maurer-Fogy, P. Jeppesen, F. Klein, A. Bird, Purification, sequence, and cellular localization of a novel chromosomal protein that binds to methylated DNA. *Cell* **69**, 905-914 (1992).
3. R. R. Meehan, J. D. Lewis, S. McKay, E. L. Kleiner, A. P. Bird, Identification of a mammalian protein that binds specifically to DNA containing methylated CpGs. *Cell* **58**, 499-507 (1989).
4. National Center for Biotechnology Information (US). Genes and Disease [Internet]. Bethesda (MD): National Center for Biotechnology Information (US); 1998-. Rett syndrome. Available from: <https://www.ncbi.nlm.nih.gov/books/NBK22188/>. Accessed July 12, 2022.
5. J. L. Neul, J. B. Lane, H. S. Lee, S. Geerts, J. O. Barrish, F. Annese, L. M. Baggett, K. Barnes, S. A. Skinner, K. J. Motil, D. G. Glaze, W. E. Kaufmann, A. K. Percy, Developmental delay in Rett syndrome: data from the natural history study. *J Neurodev Disord* **6**, 20 (2014).
6. F. F. Operto, R. Mazza, G. M. G. Pastorino, A. Verrotti, G. Coppola, Epilepsy and genetic in Rett syndrome: A review. *Brain Behav* **9**, e01250 (2019).
7. J. L. Neul, W. E. Kaufmann, D. G. Glaze, J. Christodoulou, A. J. Clarke, N. Bahi-Buisson, H. Leonard, M. E. Bailey, N. C. Schanen, M. Zappella, A. Renieri, P. Huppke, A. K. Percy, C. RettSearch, Rett syndrome: revised diagnostic criteria and nomenclature. *Ann Neurol* **68**, 944-950 (2010).
8. J. L. Neul, A. K. Percy, T. A. Benke, E. M. Berry-Kravis, D. G. Glaze, E. D. Marsh, T. Lin, S. Stankovic, K. M. Bishop, J. M. Youakim, Trofinetide for the treatment of Rett syndrome: a randomized phase 3 study. *Nat Med* **29**, 1468-1475 (2023).
9. D. Armstrong, J. K. Dunn, B. Antalffy, R. Trivedi, Selective dendritic alterations in the cortex of Rett syndrome. *J Neuropathol Exp Neurol* **54**, 195-201 (1995).
10. A. J. Sandweiss, V. L. Brandt, H. Y. Zoghbi, Advances in understanding of Rett syndrome and MECP2 duplication syndrome: prospects for future therapies. *Lancet Neurol* **19**, 689-698 (2020).
11. S. U. Peters, C. Fu, E. D. Marsh, T. A. Benke, B. Suter, S. A. Skinner, D. N. Lieberman, S. Standridge, M. Jones, A. Beisang, T. Feyma, P. Heydeman, R. Ryther, D. G. Glaze, A. K. Percy, J. L. Neul, Phenotypic features in MECP2 duplication syndrome: Effects of age. *Am J Med Genet A* **185**, 362-369 (2021).
12. J. Guy, B. Hendrich, M. Holmes, J. E. Martin, A. Bird, A mouse Mecp2-null mutation causes neurological symptoms that mimic Rett syndrome. *Nat Genet* **27**, 322-326 (2001).
13. P. D. Ross, J. Guy, J. Selfridge, B. Kamal, N. Bahey, K. E. Tanner, T. H. Gillingwater, R. A. Jones, C. M. Loughrey, C. S. McCarroll, M. E. Bailey, A. Bird, S. Cobb, Exclusive expression of MeCP2 in the nervous system distinguishes between brain and peripheral Rett syndrome-like phenotypes. *Hum Mol Genet* **25**, 4389-4404 (2016).
14. R. Z. Chen, S. Akbarian, M. Tudor, R. Jaenisch, Deficiency of methyl-CpG binding protein-2 in CNS neurons results in a Rett-like phenotype in mice. *Nat Genet* **27**, 327-331 (2001).
15. J. Guy, J. Gan, J. Selfridge, S. Cobb, A. Bird, Reversal of neurological defects in a mouse model of Rett syndrome. *Science* **315**, 1143-1147 (2007).

16. M. Lang, R. G. Wither, S. Colic, C. Wu, P. P. Monnier, B. L. Bardakjian, L. Zhang, J. H. Eubanks, Rescue of behavioral and EEG deficits in male and female *Mecp2*-deficient mice by delayed *Mecp2* gene reactivation. *Hum Mol Genet* **23**, 303-318 (2014).
17. L. Robinson, J. Guy, L. McKay, E. Brockett, R. C. Spike, J. Selfridge, D. De Sousa, C. Merusi, G. Riedel, A. Bird, S. R. Cobb, Morphological and functional reversal of phenotypes in a mouse model of Rett syndrome. *Brain* **135**, 2699-2710 (2012).
18. A. L. Collins, J. M. Levenson, A. P. Vilaythong, R. Richman, D. L. Armstrong, J. L. Noebels, J. David Sweatt, H. Y. Zoghbi, Mild overexpression of MeCP2 causes a progressive neurological disorder in mice. *Hum Mol Genet* **13**, 2679-2689 (2004).
19. M. V. Koerner, L. FitzPatrick, J. Selfridge, J. Guy, D. De Sousa, R. Tillotson, A. Kerr, Z. Sun, M. A. Lazar, M. J. Lyst, A. Bird, Toxicity of overexpressed MeCP2 is independent of HDAC3 activity. *Genes Dev* **32**, 1514-1524 (2018).
20. E. S. Na, E. D. Nelson, M. Adachi, A. E. Autry, M. A. Mahgoub, E. T. Kavalali, L. M. Monteggia, A mouse model for MeCP2 duplication syndrome: MeCP2 overexpression impairs learning and memory and synaptic transmission. *J Neurosci* **32**, 3109-3117 (2012).
21. K. K. E. Gadalla, T. Vudhironarit, R. D. Hector, S. Sinnett, N. G. Bahey, M. E. S. Bailey, S. J. Gray, S. R. Cobb, Development of a Novel AAV Gene Therapy Cassette with Improved Safety Features and Efficacy in a Mouse Model of Rett Syndrome. *Mol Ther Methods Clin Dev* **5**, 180-190 (2017).
22. S. E. Sinnett, R. D. Hector, K. K. E. Gadalla, C. Heindel, D. Chen, V. Zaric, M. E. S. Bailey, S. R. Cobb, S. J. Gray, Improved MECP2 Gene Therapy Extends the Survival of MeCP2-Null Mice without Apparent Toxicity after Intracisternal Delivery. *Mol Ther Methods Clin Dev* **5**, 106-115 (2017).
23. V. Matagne, E. Borloz, Y. Ehinger, L. Saidi, L. Villard, J. C. Roux, Severe offtarget effects following intravenous delivery of AAV9-MECP2 in a female mouse model of Rett syndrome. *Neurobiol Dis* **149**, 105235 (2021).
24. T. J. Strovas, A. B. Rosenberg, B. E. Kuypers, R. A. Muscat, G. Seelig, MicroRNA-based single-gene circuits buffer protein synthesis rates against perturbations. *ACS Synth Biol* **3**, 324-331 (2014).
25. G. Lillacci, Y. Benenson, M. Khammash, Synthetic control systems for high performance gene expression in mammalian cells. *Nucleic Acids Res* **46**, 9855-9863 (2018).
26. C. Hinderer, N. Katz, E. L. Buza, C. Dyer, T. Goode, P. Bell, L. K. Richman, J. M. Wilson, Severe Toxicity in Nonhuman Primates and Piglets Following High-Dose Intravenous Administration of an Adeno-Associated Virus Vector Expressing Human SMN. *Hum Gene Ther* **29**, 285-298 (2018).
27. J. H. Choi, N. K. Yu, G. C. Baek, J. Bakes, D. Seo, H. J. Nam, S. H. Baek, C. S. Lim, Y. S. Lee, B. K. Kaang, Optimization of AAV expression cassettes to improve packaging capacity and transgene expression in neurons. *Mol Brain* **7**, 17 (2014).
28. R. Tillotson, J. Selfridge, M. V. Koerner, K. K. E. Gadalla, J. Guy, D. De Sousa, R. D. Hector, S. R. Cobb, A. Bird, Radically truncated MeCP2 rescues Rett syndrome-like neurological defects. *Nature* **550**, 398-401 (2017).
29. J. Hordeaux, E. L. Buza, B. Jeffrey, C. Song, T. Jahan, Y. Yuan, Y. Zhu, P. Bell, M. Li, J. A. Chichester, R. Calcedo, J. M. Wilson, MicroRNA-mediated inhibition of transgene expression reduces dorsal root ganglion toxicity by AAV vectors in primates. *Sci Transl Med* **12**, (2020).

30. J. Hordeaux, Q. Wang, N. Katz, E. L. Buza, P. Bell, J. M. Wilson, The Neurotropic Properties of AAV-PHP.B Are Limited to C57BL/6J Mice. *Mol Ther* **26**, 664-668 (2018).
31. C. Huichalaf, T. L. Perfitt, A. Kuperman, R. Gooch, R. C. Kovi, K. A. Brenneman, X. Chen, D. Hirehallur-Shanthappa, T. Ma, B. T. Assaf, I. Pardo, T. Franks, L. Monarski, T. W. Cheng, K. Le, C. Su, S. Somanathan, L. O. Whiteley, C. Bulawa, M. J. Pregel, A. Martelli, In vivo overexpression of frataxin causes toxicity mediated by iron-sulfur cluster deficiency. *Mol Ther Methods Clin Dev* **24**, 367-378 (2022).
32. M. Van Alstyne, I. Tattoli, N. Delestree, Y. Recinos, E. Workman, L. S. Shihabuddin, C. Zhang, G. Z. Mentis, L. Pellizzoni, Gain of toxic function by long-term AAV9-mediated SMN overexpression in the sensorimotor circuit. *Nat Neurosci* **24**, 930-940 (2021).
33. C. M. Buchovecky, S. D. Turley, H. M. Brown, S. M. Kyle, J. G. McDonald, B. Liu, A. A. Pieper, W. Huang, D. M. Katz, D. W. Russell, J. Shendure, M. J. Justice, A suppressor screen in *Mecp2* mutant mice implicates cholesterol metabolism in Rett syndrome. *Nat Genet* **45**, 1013-1020 (2013).
34. C. A. Chapleau, E. M. Boggio, G. Calfa, A. K. Percy, M. Giustetto, L. Pozzo-Miller, Hippocampal CA1 pyramidal neurons of *Mecp2* mutant mice show a dendritic spine phenotype only in the presymptomatic stage. *Neural Plast* **2012**, 976164 (2012).
35. C. De Felice, F. Della Ragione, C. Signorini, S. Leoncini, A. Pecorelli, L. Ciccoli, F. Scalabri, F. Marracino, M. Madonna, G. Belmonte, L. Ricceri, B. De Filippis, G. Laviola, G. Valacchi, T. Durand, J. M. Galano, C. Oger, A. Guy, V. Bultel-Ponce, J. Guy, S. Filosa, J. Hayek, M. D'Esposito, Oxidative brain damage in *Mecp2*-mutant murine models of Rett syndrome. *Neurobiol Dis* **68**, 66-77 (2014).
36. N. Lozovaya, R. Nardou, R. Tyzio, M. Chiesa, A. Pons-Bennaceur, S. Eftekhari, T. T. Bui, M. Billon-Grand, J. Rasero, P. Bonifazi, D. Guimond, J. L. Gaiarsa, D. C. Ferrari, Y. Ben-Ari, Early alterations in a mouse model of Rett syndrome: the GABA developmental shift is abolished at birth. *Sci Rep* **9**, 9276 (2019).
37. M. Santos, A. Silva-Fernandes, P. Oliveira, N. Sousa, P. Maciel, Evidence for abnormal early development in a mouse model of Rett syndrome. *Genes Brain Behav* **6**, 277-286 (2007).
38. B. C. Ward, N. H. Kolodny, N. Nag, J. E. Berger-Sweeney, Neurochemical changes in a mouse model of Rett syndrome: changes over time and in response to perinatal choline nutritional supplementation. *J Neurochem* **108**, 361-371 (2009).
39. P. R. Konkalmatt, R. J. Beyers, D. M. O'Connor, Y. Xu, M. E. Seaman, B. A. French, Cardiac-selective expression of extracellular superoxide dismutase after systemic injection of adeno-associated virus 9 protects the heart against post-myocardial infarction left ventricular remodeling. *Circ Cardiovasc Imaging* **6**, 478-486 (2013).
40. K. M. Prasad, R. S. Smith, Y. Xu, B. A. French, A single direct injection into the left ventricular wall of an adeno-associated virus 9 (AAV9) vector expressing extracellular superoxide dismutase from the cardiac troponin-T promoter protects mice against myocardial infarction. *J Gene Med* **13**, 333-341 (2011).
41. C. Yang, W. H. Yang, S. S. Chen, B. F. Ma, B. Li, T. Lu, T. Y. Qu, R. L. Klein, L. R. Zhao, W. M. Duan, Pre-immunization with an intramuscular injection of AAV9-human erythropoietin vectors reduces the vector-mediated transduction following re-administration in rat brain. *PLoS One* **8**, e63876 (2013).
42. K. K. Gadalla, M. E. Bailey, R. C. Spike, P. D. Ross, K. T. Woodard, S. N. Kalburgi, L. Bachaboina, J. V. Deng, A. E. West, R. J. Samulski, S. J. Gray, S. R. Cobb, Improved survival and reduced phenotypic severity following AAV9/MECP2 gene

- transfer to neonatal and juvenile male *Mecp2* knockout mice. *Mol Ther* **21**, 18-30 (2013).
43. S. K. Garg, D. T. Lioy, H. Cheval, J. C. McGann, J. M. Bissonnette, M. J. Murtha, K. D. Foust, B. K. Kaspar, A. Bird, G. Mandel, Systemic delivery of MeCP2 rescues behavioral and cellular deficits in female mouse models of Rett syndrome. *J Neurosci* **33**, 13612-13620 (2013).
 44. M. Luoni, S. Giannelli, M. T. Indrigo, A. Niro, L. Massimino, A. Iannielli, L. Passeri, F. Russo, G. Morabito, P. Calamita, S. Gregori, B. Deverman, V. Broccoli, Whole brain delivery of an instability-prone *Mecp2* transgene improves behavioral and molecular pathological defects in mouse models of Rett syndrome. *Elife* **9**, (2020).
 45. S. Powers, S. Likhite, K. K. Gadalla, C. J. Miranda, A. J. Huffenberger, C. Dennys, K. D. Foust, P. Morales, C. R. Pierson, F. Rinaldi, S. Perry, B. Bolon, N. Wein, S. Cobb, B. K. Kaspar, K. C. Meyer, Novel MECP2 gene therapy is effective in a multicenter study using two mouse models of Rett syndrome and is safe in non-human primates. *Mol Ther* **31**, 2767-2782 (2023).
 46. S. E. Sinnett, E. Boyle, C. Lyons, S. J. Gray, Engineered microRNA-based regulatory element permits safe high-dose miniMECP2 gene therapy in Rett mice. *Brain* **144**, 3005-3019 (2021).
 47. C. Sadhu, C. Lyons, J. Oh, I. Jagadeeswaran, S. J. Gray, S. E. Sinnett, The Efficacy of a Human-Ready miniMECP2 Gene Therapy in a Pre-Clinical Model of Rett Syndrome. *Genes (Basel)* **15**, (2023).
 48. V. Matagne, Y. Ehinger, L. Saidi, A. Borges-Correia, M. Barkats, M. Bartoli, L. Villard, J. C. Roux, A codon-optimized *Mecp2* transgene corrects breathing deficits and improves survival in a mouse model of Rett syndrome. *Neurobiol Dis* **99**, 1-11 (2017).
 49. V. Matagne, S. Budden, S. R. Ojeda, J. Raber, Correcting deregulated *Fxyd1* expression ameliorates a behavioral impairment in a mouse model of Rett syndrome. *Brain Res* **1496**, 104-114 (2013).
 50. S. Luikenhuis, E. Giacometti, C. F. Beard, R. Jaenisch, Expression of MeCP2 in postmitotic neurons rescues Rett syndrome in mice. *Proc Natl Acad Sci U S A* **101**, 6033-6038 (2004).
 51. D. X. Bharucha-Goebel, J. J. Todd, D. Saade, G. Norato, M. Jain, T. Lehky, R. M. Bailey, J. A. Chichester, R. Calcedo, D. Armao, A. R. Foley, P. Mohassel, E. Tesfaye, B. P. Carlin, B. Seremula, M. Waite, W. M. Zein, L. A. Huryn, T. O. Crawford, C. J. Sumner, A. Hoke, J. D. Heiss, L. Charnas, J. E. Hooper, T. W. Bouldin, E. M. Kang, D. Rybin, S. J. Gray, C. G. Bonnemann, G. A. N. T. Team, Intrathecal Gene Therapy for Giant Axonal Neuropathy. *N Engl J Med* **390**, 1092-1104 (2024).
 52. C. Schmitt-Ulms, A. Kayabolen, M. Manero-Carranza, N. Zhou, K. Donnelly, S. P. Nuccio, K. Kato, H. Nishimasu, J. S. Gootenberg, O. O. Abudayyeh, Programmable RNA writing with trans-splicing. *bioRxiv*, (2024).
 53. J. R. Sinnamon, M. E. Jacobson, J. F. Yung, J. R. Fisk, S. Jeng, S. K. McWeeney, L. K. Parmelee, C. N. Chan, S. P. Yee, G. Mandel, Targeted RNA editing in brainstem alleviates respiratory dysfunction in a mouse model of Rett syndrome. *Proc Natl Acad Sci U S A* **119**, e2206053119 (2022).
 54. J. R. Sinnamon, S. Y. Kim, G. M. Corson, Z. Song, H. Nakai, J. P. Adelman, G. Mandel, Site-directed RNA repair of endogenous *Mecp2* RNA in neurons. *Proc Natl Acad Sci U S A* **114**, E9395-E9402 (2017).
 55. A. Martella, M. Matjusaitis, J. Auxillos, S. M. Pollard, Y. Cai, EMMA: An Extensible Mammalian Modular Assembly Toolkit for the Rapid Design and Production of Diverse Expression Vectors. *ACS Synth Biol* **6**, 1380-1392 (2017).

56. P. Bankhead, M. B. Loughrey, J. A. Fernandez, Y. Dombrowski, D. G. McArt, P. D. Dunne, S. McQuaid, R. T. Gray, L. J. Murray, H. G. Coleman, J. A. James, M. Salto-Tellez, P. W. Hamilton, QuPath: Open source software for digital pathology image analysis. *Sci Rep* **7**, 16878 (2017).

Acknowledgments: The authors thank Amanda Morris, Gwen Tsang, Scott Noble, Wonsuk Lee, Elisa Hall-Ponsele, Adam Mol, Sussan Rosser, Stephanie Mearns, and Mark Bailey for early discussions. We thank Jacky Guy and Julie Jordan for comments on the manuscript. We thank Premier Laboratory for the mouse histopathology sample preparation. Medical writing and editorial support were provided by Marjet Heitzer of 360 Medical Writing and funded by Neurogene Inc.

Funding: This study was funded by Neurogene Inc., with additional laboratory support from the Simons Initiative for the Developing Brain and the Rett Syndrome Research Trust.

Author contributions: Author contributions conform to the ICMJE guidelines for authorship.

Conceptualization: S.R.C., P.D.R., R.D.H., S.R.B., R.M.

Methodology: P.D.R., R.D.H., K.K.E.G., J.S., S.R.T., J.B., B.B.

Investigation: P.D.R., R.D.H., K.K.E.G., J.S., S.R.T., J.B., B.B.

Visualization: S.R.C., P.D.R., R.D.H., J.S., S.R.T.

Funding acquisition: S.R.C.

Project administration: S.R.C., P.D.R., S.R.B.

Supervision: S.R.B.

Writing – original draft: S.R.C., P.D.R., R.D.H., J.S., S.R.B., R.M.

Writing – review & editing: All authors

Competing interests: SRC is Chief Scientific Officer, RM is Founder and Chief Executive Officer, and SRB is Senior Director of Preclinical Development at Neurogene Inc. where they have equity interest. SRC, PDR and RDH are co-inventors on patents WO/2022/003348 (Transgene Expression System) and WO/2023/144565 (Recombinant Optimized MECP2 Cassettes and Methods for Treating Rett Syndrome and Related Disorders) which have been licensed to Neurogene Inc. The other authors declare that they have no competing interests.

Data and materials availability: All data associated with this study are present in the paper or supplementary materials. The sequences for the constructs used in the study are included in Data file S2. The raw data for experiments where $n < 20$ is provided in Data file S4. RNA-seq data is available through GEO (accession number GSEXXXX).

Figure legends

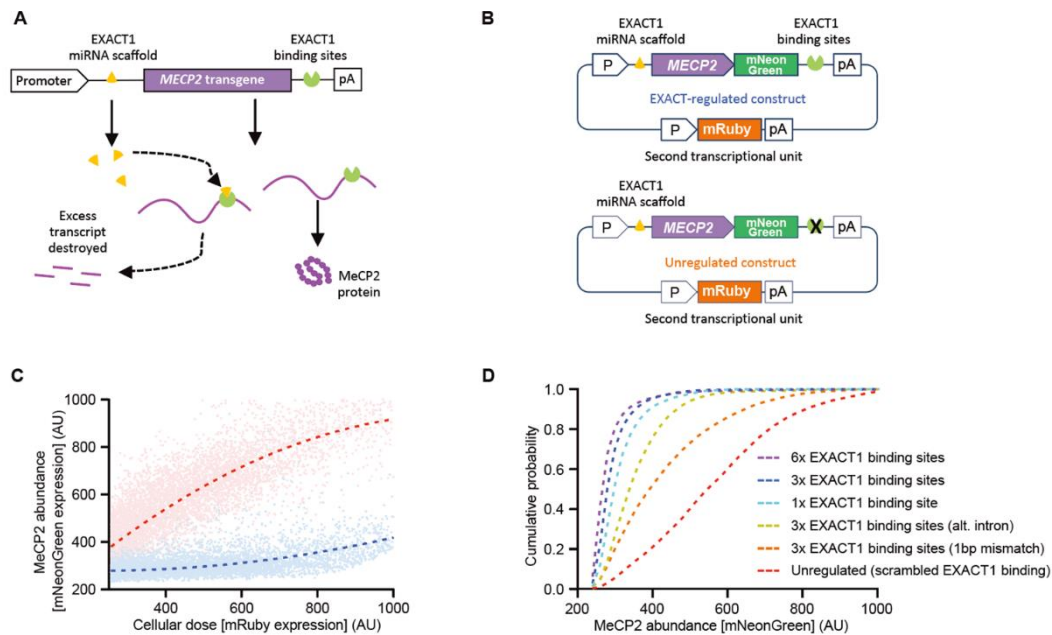


Fig. 1. EXACT regulates *MECP2* transgene expression in vitro. (A) Schematic showing the structure of the EXACT-*MECP2* construct and control of *MECP2* expression. The *MECP2* transgene (purple) is transcribed into mRNA (transcripts indicated by purple lines) that contain EXACT1 microRNA binding sites in the 3'UTR (green symbols). A proportion of mRNA is translated into full-length MeCP2 protein (right), but to avoid overexpression, EXACT1 miRNA (yellow triangles) is co-transcribed in proportion to the transgene and binds to the EXACT1 binding sites in the *MECP2* transcripts, leading to the destruction of excess transcripts (left). (B) Schematic showing the plasmid constructs used for in vitro analysis. In the top construct, the *MECP2*-mNeonGreen fusion cassette is followed by EXACT1 binding sites, allowing EXACT regulation, whereas the bottom construct does not contain EXACT1 binding sites. All constructs expressed mRuby from a second transcriptional unit on the plasmid as a measure of cellular dose. (C) Plot displaying flow cytometry data of HEK293A cells transfected with varying doses of plasmids containing either of the two constructs shown in 1B. The Y axis displays mNeonGreen expression (AU) as a representation of transgene expression; the X axis displays mRuby expression (AU) as a representation of plasmid dose received by the cell. Dark blue represents the EXACT1 construct (EXACT-regulated construct containing 3× binding sites in the 3'UTR, schematic shown in Fig. 1B, top), and red represents the unregulated construct (schematic shown in Fig. 1B, bottom). (D) Cumulative probability plot of flow cytometry data comparing the proportion of cells with MeCP2-NeonGreen protein expression across different versions of the regulated circuit. Modifying individual elements of the circuit allows the regulation to be tuned to the appropriate level, with more highly regulated circuits leading to more restrained protein expression.

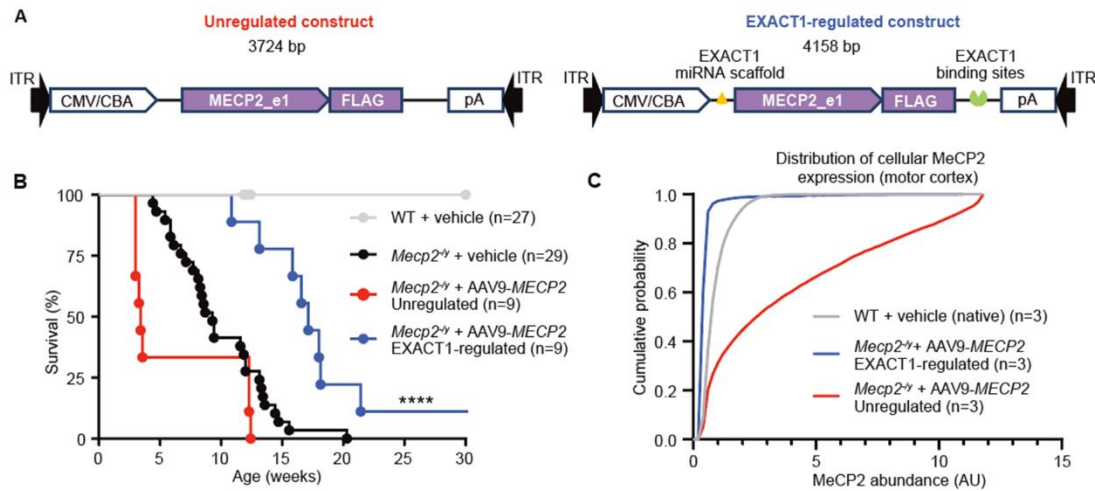


Fig. 2. Survival and cellular expression studies using a first-generation EXACT-MECP2 vector in *Mecp2*^{-/-} mice. (A) Schema of the unregulated and EXACT-regulated vectors assessed in *Mecp2*^{-/-} mice. The CMV/CBA promoter drives expression of a human *MECP2* transgene (e1 isoform), which is FLAG-tagged at the C-terminus. AAV2 inverted terminal repeats (ITRs; displayed as black arrows) flank the single-stranded AAV vector genomes (vg). The unregulated construct is shown on the left, and the EXACT-regulated construct is shown on the right. (B) Kaplan-Meier plot showing survival of vector-treated (3×10^{11} vg/mouse) and vehicle-dosed *Mecp2*^{-/-} mouse cohorts (**** p < 0.0001 Mantel-Cox test versus vehicle-dosed *Mecp2*^{-/-} mice). Due to rolling enrollment of wild-type (WT) mice, some WT mice had not yet reached the 30-week time point by the end of the study. Group sizes were as follows: WT + vehicle, n=27; *Mecp2*^{-/-} + vehicle, n=29; *Mecp2*^{-/-} + AAV9-MECP2 unregulated, n=9; *Mecp2*^{-/-} + AAV9-MECP2 EXACT-regulated, n=9. (C) Cumulative probability plot of anti-MeCP2 immunofluorescence signal in cells of the motor cortex in *Mecp2*^{-/-} mice treated with either unregulated or EXACT-regulated constructs or in control WT mice treated with vehicle.. AU = arbitrary units. Group sizes were as follows: WT + vehicle, n=3; *Mecp2*^{-/-} + AAV9-MECP2 unregulated, n=3; *Mecp2*^{-/-} + AAV9-MECP2 EXACT-regulated, n=3.

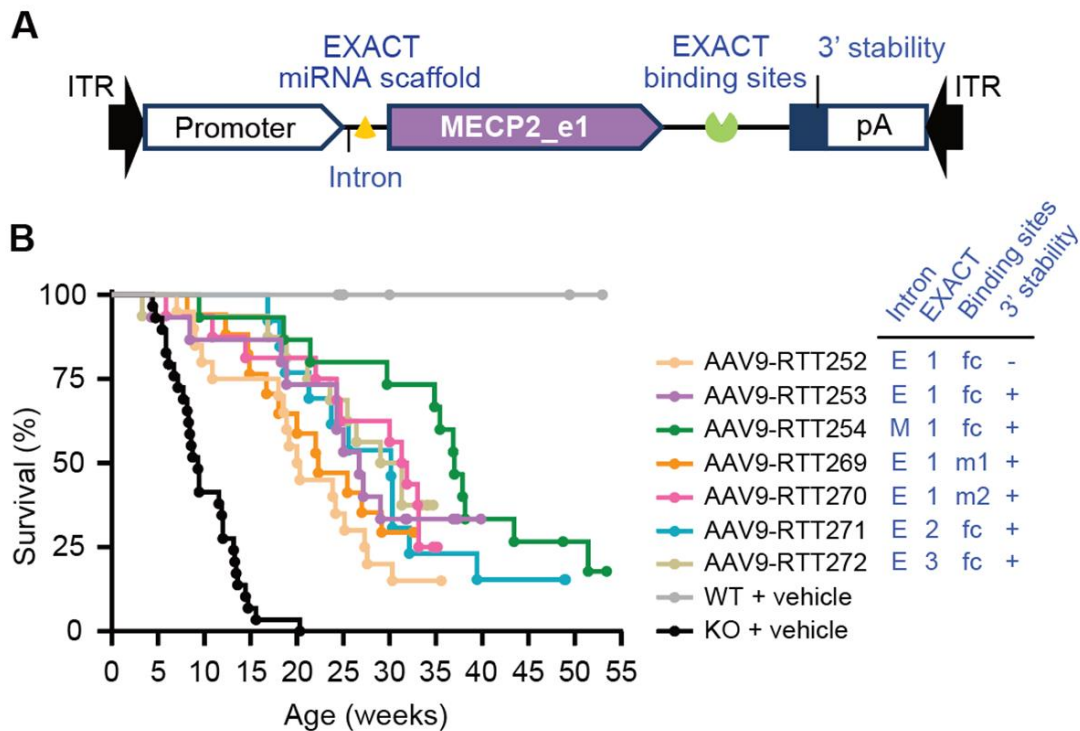


Fig. 3. Survival and clinical score in construct selection efficacy study. (A) Schematic showing elements of the EXACT construct that were tested in construct selection efficacy study. Elements highlighted in blue text were systematically modified and tested in *Mecp2^{-y}* mice. (B) Kaplan-Meier plot showing survival of vector-treated (3×10^{11} vg/mouse) and vehicle-dosed *Mecp2^{-y}* mouse cohorts (all $p < 0.0001$ for vector-treated versus vehicle-dosed *Mecp2^{-y}* mice, Mantel-Cox test). Group sizes were as follows: WT + Vehicle, $n=27$; KO + Vehicle, $n=30$; KO + AAV9-RTT252, $n=20$; KO + AAV9-RTT253, $n=15$; KO + AAV9-RTT254, $n=15$; KO + AAV9-RTT269, $n=17$; KO + AAV9-RTT270, $n=16$; KO + AAV9-RTT271, $n=13$; KO + AAV9-RTT272, $n=16$. Genetic elements in each construct are detailed in blue text: intron is EF1a (E) or MINX (M); EXACT specifies the miRNA scaffold expressing EXACT1 miRNA (1), EXACT2 miRNA (2) or EXACT3 miRNA (3); sites specifies if the EXACT binding sites are fully complementary (fc) or contain a single nucleotide mismatch (m1/m2); stability element is present (+) or absent (-) in the 3'UTR.

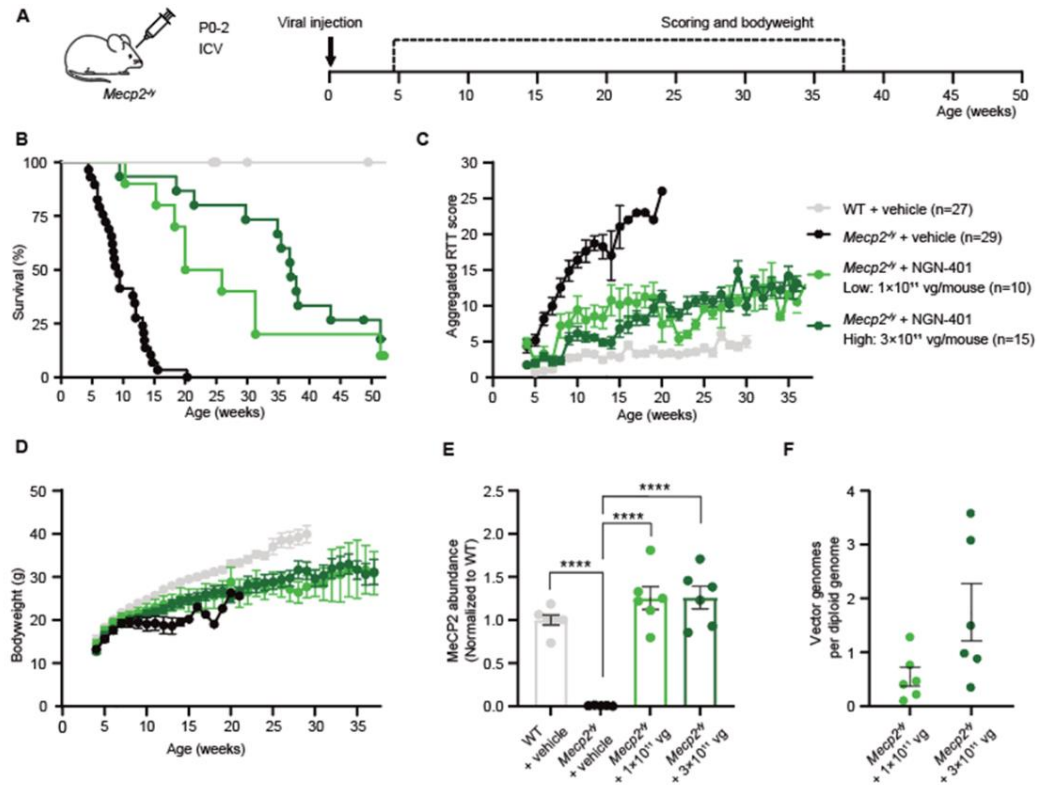


Fig. 4. Efficacy of NGN-401 in *Mecp2*^{-/-} mice. (A) Schematic showing the study design and timeline. (B) Kaplan-Meier plot showing survival of the vehicle- and vector-dosed *Mecp2*^{-/-} cohorts (all $p < 0.0001$ for NGN-401-treated versus vehicle-dosed *Mecp2*^{-/-} mice, Mantel-Cox test). Group sizes were as follows: wild-type (WT) + Vehicle, $n=27$; *Mecp2*^{-/-} + Vehicle, $n=29$; *Mecp2*^{-/-} + NGN-401 1×10^{11} vg/mouse, $n=10$; *Mecp2*^{-/-} + NGN-401 3×10^{11} vg/mouse, $n=15$. Due to rolling enrollment of WT mice, some WT mice had not yet reached the 30-week time point by the end of the study. (C) The aggregated RTT phenotype score (produced by adding the scores for six parameters graded individually on a scale from 0-5 [see fig. S2 and Table S1]), and (D) body weights for animals in (B) plotted out to median survival point for the high dose cohort. Again, due to rolling enrollment of WT mice, some WT mice had not yet reached the 30-week time point by the end of the study. (E) Plot showing MeCP2 abundance in the cortex of the indicated groups, relative to WT animals treated with vehicle. Group sizes were as follows: WT + vehicle, $n=5$; *Mecp2*^{-/-} + vehicle, $n=6$; *Mecp2*^{-/-} + NGN-401 1×10^{11} vg/mouse, $n=6$; *Mecp2*^{-/-} + NGN-401 3×10^{11} vg/mouse, $n=6$ (one-way ANOVA; **** $p < 0.0001$; Tukey's multiple comparison test). Protein abundance was assessed by Western blot. MeCP2 abundance is shown relative to WT by normalizing MeCP2 expression to endogenous MeCP2 abundance in the WT + vehicle cohort (F) vector genome quantification in the cerebral cortex of low- and high-dose-treated *Mecp2*^{-/-} mice (assessed by qPCR, 8 weeks after dosing; $n=6$ per group). Vector genomes are shown as vector genomes per diploid genome by normalizing vector copy numbers to mouse *Actb* copy numbers.

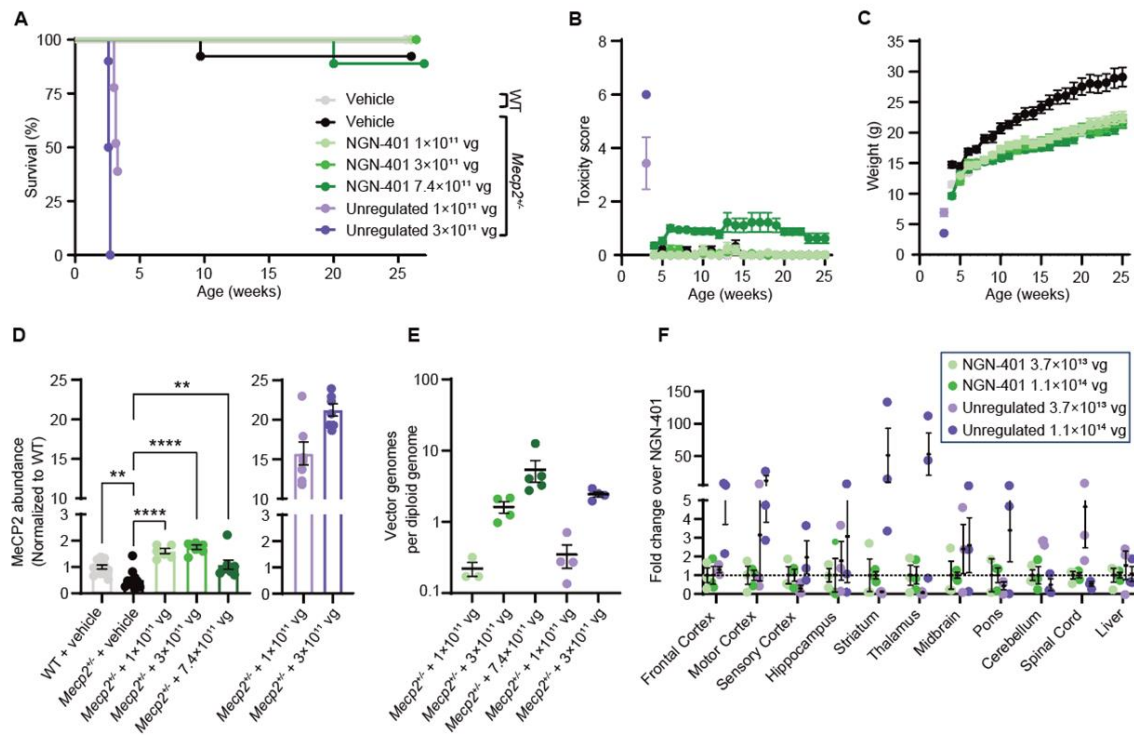


Fig. 5. NGN-401 is well tolerated and provides controlled expression in *Mecp2*^{+/-} mice and nonhuman primates. (A) Kaplan-Meier plot showing survival curves for vehicle-treated wild-type and *Mecp2*^{+/-} mice, as well as *Mecp2*^{+/-} mice treated with one of three doses of NGN-401 or one of two doses of unregulated vector. (B and C) Toxicity scores (B) and (C) body weights for wild-type and *Mecp2*^{+/-} vehicle-treated and vector-dosed animals studied in 5A. Group sizes were as follows: WT + Vehicle, n=20; *Mecp2*^{+/-} + Vehicle, n=13; *Mecp2*^{+/-} + NGN-401 1×10¹¹ vg/mouse, n=13; *Mecp2*^{+/-} + NGN-401 3×10¹¹ vg/mouse, n=17; *Mecp2*^{+/-} + NGN-401 7.4×10¹¹ vg/mouse, n=9; *Mecp2*^{+/-} + Unregulated 1×10¹¹ vg/mouse, n=10; *Mecp2*^{+/-} + Unregulated 3×10¹¹ vg/mouse, n=9. The two groups treated with unregulated vector were euthanized early due to severe toxicity. (D) Plot showing MeCP2 abundance in the cortex of the indicated groups, relative to WT animals treated with vehicle. Group sizes were as follows: WT + vehicle, n=5; *Mecp2*^{+/-} + vehicle, n=5; *Mecp2*^{+/-} + NGN-401 1×10¹¹ vg/mouse, n=6; *Mecp2*^{+/-} + NGN-401 3×10¹¹ vg/mouse, n=6; *Mecp2*^{+/-} + 7.4×10¹¹ vg/mouse, n=8; *Mecp2*^{+/-} + Unregulated 1×10¹¹ vg/mouse, n=7; *Mecp2*^{+/-} + Unregulated 3×10¹¹ vg/mouse, n=7. Protein abundance was assessed by Western blot (one-way ANOVA; **** p < 0.0001; Tukey's multiple comparison test). (E) Plot quantifying vector genomes in the cerebral cortex of treated animals in the indicated groups, as assessed by qPCR. Animals treated with 1×10¹¹ (n=3), 3×10¹¹ (n=4), or 7.4×10¹¹ (n=5) vg/mouse of NGN-401 were assessed at 26 weeks post dosing, and animals treated with 1×10¹¹ (n=4) or 3×10¹¹ (n=4) vg/mouse of unregulated vector were assessed at 8 and 2 weeks post-dosing, respectively. Vector genomes are shown as vector genomes per diploid genome by normalizing vector copy numbers to mouse *Actb* copy numbers. (F) Plot showing relative mRNA expression in the indicated tissues from nonhuman primate study comparing selected neural tissues and liver from animals treated with NGN-401 or unregulated *MECP2* vector at 3.7×10¹³ or 1.1×10¹⁴ vg per animal, evaluated at 29/30 days after dosing. (n=3 animals/group).